AIAA 99-0925

Oscillatory Excitation of Unsteady Compressible Flows over Airfoils at Flight Reynolds Numbers

Avi Seifert and LaTunia G. Pack

NASA Langley Research Center

Hampton, VA

37th AIAA Aerospace Sciences Meeting and Exhibit

January 11-14, 1999/ Reno, NV

Oscillatory Excitation of Unsteady Compressible Flows over Airfoils at Flight Reynolds Numbers

Avi Seifert* **and LaTunia G. Pack†**
Flow Modeling and Control Branch, NASA Langley Research Center
Hampton, Va. 23681-0001

Abstract

An experimental investigation, aimed at delaying flow separation due to the occurrence of a shock-wave-boundary-layer interaction, is reported. The experiment was performed using a NACA 0012 airfoil and a NACA 0015 airfoil at high Reynolds number incompressible and compressible flow conditions. The effects of Mach and Reynolds numbers were identified, using the capabilities of the cryogenic-pressurized facility to maintain one parameter fixed and change the other. Significant Reynolds number effects were identified in the baseline compressible flow conditions even at Reynolds number of 10 and 20 million. The main objectives of the experiment were to study the effects of periodic excitation on airfoil drag-divergence and to alleviate the severe unsteadiness associated with shock-induced separation (known as "buffeting"). Zero-mass-flux oscillatory blowing was introduced through a downstream directed slot located at 10% chord on the upper surface of the NACA 0015 airfoil. The effective frequencies generated 2-4 vortices over the separated region, regardless of the Mach number. Even though the excitation was introduced upstream of the shock-wave, due to experimental limitations, it had pronounced effects downstream of it. Wake deficit (associated with drag) and unsteadiness (associated with buffeting) were significantly reduced. The spectral content of the wake pressure fluctuations indicates of steadier flow throughout the frequency range when excitation was applied. This is especially important at low frequencies which are more likely to interact with the airframe.

Nomenclature

a	speed of sound, $\equiv \sqrt{\gamma RT}$
$\langle c_\mu \rangle$	oscillatory blowing momentum coefficient, $\equiv h/c\left(1 + T_\infty / T_j\right)\left(\langle u' \rangle / U_\infty\right)^2$
c	airfoil chord
C_d	total drag coefficient
C_{dp}	form drag coefficient
C_{do}	zero-lift drag coefficient
C_l	lift coefficient
C_p	pressure coefficient, $\equiv \left(P - P_s\right)/q$
C_p'	fluctuating pressure coefficient, $\equiv p'/q$
f	frequency [Hz]
GN_2	gaseous nitrogen
F^+	reduced frequency, $\equiv fX_{te} / U_\infty$
h	slot height or width
M	Mach number, $\equiv U_\infty / a$
P	pressure
q	free stream dynamic pressure, $\equiv 1/2 \rho U_\infty^2$
R_c	chord Reynolds number, $\equiv U_\infty c / \nu$
T	temperature
U, u	averaged and fluctuating velocity
X/c	normalized streamwise location
X_{te}	distance from actuator to TE
Y/c	distance normal to airfoil surface
Z	spanwise location
α	airfoil angle of attack, deg
ν	kinematic viscosity
ρ	density

Abbreviations

LE	airfoil leading edge
TE	airfoil trailing edge
< >	phase locked values

Subscripts

j	conditions at blowing slot
max	conditions at maximum lift
s	tunnel static conditions
∞	free stream conditions

Superscripts

'	root mean square of fluctuating value
crit	critical Mach number
res	acoustic resonance frequency

---

* NRC researcher, on leave from Tel-Aviv University, member AIAA.
† Research engineer, Flow Modeling and Control Branch.

1. Introduction

Low Reynolds and Mach number studies [Ref. 1-3 and references therein] have shown that periodic vortical excitation introduced into a separating boundary layer, slightly upstream of the average separation location, can effectively delay boundary layer separation. The improved ability of the boundary layer to overcome an adverse pressure gradient is attributed to enhanced mixing between the low momentum fluid near the wall and the external high momentum flow. The successful application of the method increases the lift while maintaining low drag. At low Mach numbers, where high-lift for take-off, landing or loiter is required, the delay of boundary layer separation allows increased loading of a multi-element high-lift airfoil system.

It was recently demonstrated[4] that periodic excitation of the boundary layer upstream of separation can delay the occurrence of the adverse effects associated with boundary layer separation and significantly enhance the performance of airfoils at flight Reynolds numbers and incompressible speeds. Low Reynolds number experiments, where control was applied from the LE region of the airfoils, were repeated at a chord Reynolds number of 37.6×10^6. Using a flapped NACA 0015 airfoil, where control was applied at the flap shoulder, it was shown that the method is essentially independent of Reynolds number[4], as long as the appropriate dimensionless control parameters are applied.

A recently published numerical simulation[5] shows that oscillatory excitation of a separated boundary layer, at low Reynolds and Mach numbers, can significantly increase post-stall lift at excitation frequencies that are 0.3 to 4 times the natural vortex shedding frequency (F^+=0.4 in this case). By using frequencies that are at least twice the shedding frequency, which correspond to our definition of $F^+ \approx 0.8$, the lift enhancement is accompanied by a significant reduction in drag and drag excursions [Fig. 6 and 7 in Ref. 5]. Indications of these effects were experimentally identified in Ref. 4. Using an appropriate combination of frequency ($F^+ \approx 1$) and magnitude ($< c_\mu >$= 10 to 50×10^{-5}) the flow should be steadier, even if it is intermittently separated. Similar trends, at least for the lift increment and the excitation F^+, were identified numerically[6]. Oscillatory addition of momentum is two orders of magnitude more efficient than tangential steady blowing for separation control[2,4]. Neither forced transition, thickened turbulent boundary layer nor elevated Reynolds numbers[4] (up to $37.6 * 10^6$ tested) had an adverse effect on the efficiency of the method. The nature of the device used to generate the unsteady disturbances is not important, as long as the end result (i.e. the vortical excitation) is similar. Two dimensional, wall tangential oscillatory blowing[2,4] is currently used since the magnitude, the frequency and the average mass flux are conveniently controllable, while the airfoil geometry is almost unchanged, due to the narrow blowing slots.

Flow separation at compressible speeds typically occurs downstream of a shock-wave/boundary-layer interaction. The pressure jump across the shock either causes immediate separation or thickens the boundary layer and reduces its momentum such that it separates further downstream. Once the flow separates downstream of the shock, the unsteady separation and subsequent reattachment (if it occurs) induce unsteadiness both in the shock position and strength. This phenomenon is known as buffeting. The low frequency oscillations can cause structural damage, if coupled with the resonance frequencies of the structure. Porous strips and wall bumps[7] are effective in reducing the strength of the shock-wave. Vortex generators (mechanical[8] or canted jets[9]) as well as suction through slots, are effective at controlling shock-induced separation and alleviating buffet.

Triangular, ramp-like, vortex generators were used in a numerical simulation to demonstrate passive control of shock-wave/boundary-layer interaction and buffet alleviation[10]. This was achieved by energizing the boundary layer upstream of the shock-wave by pairs of counter rotating vortices. The vortices were generated 15 boundary layer thicknesses (50 devices heights) *upstream* of the shock position. Although placed upstream, the main effect was a smaller separation bubble *downstream* of the shock. As a result of the thinner boundary layer the shock strength increased, as did the rate of pressure recovery downstream of it. The calculated pressures are in qualitative agreement with experiment[8]. Additional aspects such as skin friction, device drag and flow unsteadiness were not investigated.

The effects of suction through slots and a porous surface, on the performance of a supercritical airfoil at off-design conditions were tested experimentally[11]. Suction through a single slot with a mass flow coefficient of 60×10^{-5} (slot width unknown therefore momentum coefficient unknown) was very effective in maintaining the upstream shock position, re-establishing the pressure recovery and positive $C_{p,TE}$, and increasing post-stall lift but was less effective in reducing drag. The double slot and perforated plate (8% porosity over 7.5% chord) were less effective than the single slot at increasing post-stall lift, but more effective in reducing drag (when using the same mass flow coefficient, i.e. significantly smaller momentum coefficient). The double slot and perforated plate were effective even without the suction. This was possible because the cavity underneath allowed mass transfer from the downstream side of the shock (high pressure) to the upstream side of it. In the steady sense, the suction downstream of the shock reduced the boundary layer tendency to separate while the upstream bleed from the surface, thickened the boundary layer and

reduced the shock strength. This in turn reduced the tendency for separation downstream. The double slot was especially effective in buffet alleviation, completely eliminating the shock-wave/separated flow coupling. The physical mechanism producing this effect was not identified.

To be efficient the above mentioned methods need to be actively controlled. Bump position, height and shape need to be tailored to each specific flow condition. Porous strips need to cover about 10% of the chord, cause transition on laminar airfoils and increase skin friction drag. Porosity and slot locations also need to be mission tailored. While these devices could be designed to widen the flight envelope to a certain extent, their application for guidance and control, which requires fast response[12], is doubtful. Furthermore, efficiency considerations rule out the use of tangential blowing and stealth considerations rule out the use of mechanical vortex generators. Therefore, fast responding, active methods for management of high-lift as well as compressible unsteady flows are studied.

The objectives of the present investigation are the following:

1. To reduce flow unsteadiness in incompressible speeds and to determine the relationship between the controlled excitation and the naturally occurring unsteady flow in the presence of separated flows.
2. To suppress shock-induced separation and provide buffet alleviation by using periodic excitation.

2. Experimental Set-up

2.1 Overview

The experiment was conducted in the 0.3-meter Transonic Cryogenic Tunnel at NASA Langley Research Center, using Gaseous Nitrogen (GN2) as the test fluid. The execution of an active flow control experiment in a pressurized cryogenic wind tunnel has advantages and disadvantages. For example, a cryogenic pressurized facility allows independent control of R_c and M at a fixed free stream velocity. With this type of control, the effective frequencies are clearly indicated because F^+ can be held fixed when R_c is varied and M is held constant or R_c is fixed while M is varied. Another advantage of testing in a cryogenic pressurized facility is the ability to generate a zero mass flux disturbance when using an oscillatory blowing valve. One of the disadvantages of testing in a cryogenic pressurized facility is that an in-situ determination of $< c_\mu >$ is very difficult. However, using atmospheric bench-top tests and a simplified flow model it is possible to estimate the $< c_\mu >$ used[4].

A new diagnostic tool was used in this experiment. It consists of a wake rake that was instrumented with dynamic pressure transducers. Its calibration and the methodology of data processing are presented in the following sections. A conventional NACA 0012 airfoil was tested in order to validate the new rake and to acquire unsteady wake data over a smaller chord, smooth airfoil. The straight NACA 0015 airfoil was tested with control applied from the LE region.

2.2 The Wind Tunnel

The experiment was conducted in the 0.3-meter Transonic Cryogenic Wind Tunnel at the NASA Langley Research Center. It is a closed loop, fan driven tunnel with a test cross section of 0.33m x 0.33m. Gaseous nitrogen (GN_2) is the test medium. The tunnel operates at stagnation pressures ranging from 1.2 bar up to 6 bar and total temperatures from 78K up to 327K [13, 14]. The floor and ceiling of the tunnel were diverged by 0.3° to 0.4° in the vicinity of the airfoil to reduce blockage resulting from boundary layer growth on the test section walls. A wake survey rod extends from the left tunnel sidewall to vertically traverse the airfoil wake (see Fig. 1). Details about the wake data acquisition system are provided in section 2.7.

Wall pressures were acquired together with the airfoil pressures at all test conditions. This information could be used later for numerical simulation of the flow taking into consideration wall interference effects.

2.3 The Airfoils

The experiments were conducted on a standard NACA 0012 airfoil (c=165 mm) and a NACA 0015 airfoil (c=254 mm). The NACA 0015 airfoil (Fig. 2) was equipped with a blowing slot at 10% chord, suitable for the control of separation near the leading edge. The slot was about 0.2% chord wide (0.5 mm), and allowed an almost tangential streamwise introduction of the excitation. Each airfoil was equipped with some 50 static pressure taps. The airfoil and test section wall pressures were recorded by the tunnel pressure scanning system.

2.4 Oscillatory Blowing System

A rotating, siren type, valve was used to generate the pressure oscillations inside the airfoil cavity. The oscillatory blowing valve was upgraded and is presently capable of generating frequencies up to 800 Hz and fluctuating pressure levels of 5 psi. For safety reasons the valve was rated to 300 psi. GN_2 was supplied to the valve by converting a portion of the liquid nitrogen available for operating the tunnel using an ambient temperature vaporizer. The use of ambient temperature GN_2 simplified the valve design. A pressure regulator controlled the GN_2 entering the valve and the variable speed drive of the valve motor controlled the frequency of the pressure oscillations. The oscillatory blowing valve was attached to the right tunnel plenum door at the center of rotation of the turntable (Fig. 1). A 49mm I.D. pipe

connected the valve to the leading edge cavity. The exhaust side of the airfoil was connected to the tunnel boundary layer removal system. The valves in the boundary layer removal system controlled the flow rate out the exhaust side of the airfoil cavity (Fig 1). Any relevant combination of steady and oscillatory blowing could be generated with this type of control. However, all the results presented in this paper are for zero-mass-flux excitation.

2.5 Bench -Top Experiments

The phase-locked pressure fluctuations (<p'>) at the entrance to the airfoil cavity were measured both in-situ and with bench-top tests. The correlation between $\langle u'^2 \rangle$ and $\langle p' \rangle/\rho$ (derived from the bench-top tests) is used to calculate the $< c_\mu >$ in the cryogenic tests[4].

The velocity fluctuations exiting the slots of the airfoil were measured with the airfoil outside the tunnel using a hot-wire mounted on a 3D traverse system. The GN_2 supplied to the oscillatory blowing valve during the wind tunnel test was replaced with compressed air. All of the pipe accessories were identical in both the wind tunnel and the bench-top experiments in order to maintain similarity between the two experiments. While any desired combination of oscillatory and steady flow rates were obtainable in the wind-tunnel experiment, steady suction could not be applied in the bench-top experiments because of the atmospheric test conditions. However, even in the bench-top experiments, reverse flow in the slot was encountered due to the instantaneous, sub-atmospheric pressures created by the inertia of the continuous flow along the airfoil cavity. The signals from the dynamic pressure transducer and the hot-wire were acquired using a 16-bit high speed A/D converter, coupled with an anti-aliasing filter. In the cases where reverse flow was expected at the slot exit, the hot-wire signal was de-rectified to account for the reverse flow[4].

2.6 The Dynamic Wake-Rake

The wake of the airfoils was traversed using the tunnel standard wake survey rake and a modified wake rake, instrumented with two dynamic pressure transducers and seven total pressure tubes. The modified wake rake enables the recording of unsteady wake data, phase locked to the controlled excitation. Its LE was machined to a semi-elliptic shape. The dynamic wake rake was located 3.1 and 2 chords downstream of the NACA 0012 and 0015 airfoils mid chord, respectively.

Fig. 3 presents a picture of the dynamic wake rake. The dynamic pressure transducers were installed inside tubes 2 and 4 of the rake. The tubes were displaced 12.7 mm in the spanwise direction, while tube #1 was located 38.1 mm from the tunnel centerline. Due to the relatively large outer diameter of the transducer (2.36mm), which could adversely affect the measurement of the wake dynamic pressure, it was decided to use a smaller diameter tube (1.60 mm O.D. and 1.03 mm), about 30 mm long, from the transducer's face to the measuring location. The length and internal volume of this tube can change the frequency response of the tube-transducer system due to acoustic resonance. A calibration was performed by placing a sound source in front of the wake rake, inside the wind tunnel test section at atmospheric conditions, with the tunnel flow off. The sound was either white noise or discrete tones. A microphone was positioned next to the tubes. The signals from the two dynamic pressure transducers were recorded along with the microphone output. These results are used to correct the signals measured under various tunnel conditions, assuming that the only variant is the flow temperature (which affects the speed of sound).

Fig. 4 presents the results of the white noise and discrete tone testing. The white noise results show that the microphone and the dynamic pressure transducer measure similar noise levels (±2dB) between 150Hz and 1KHz. The discrete tone testing was performed at a resolution of about 100 Hz and at significantly higher SPL levels (about 104 dB) than the white noise test. Figure 4 also presents the SPL difference between the dynamic pressure transducer and the microphone. Transducer #1 (position #2 in the wake-rake see Fig. 3) and the microphone measure similar SPL until 0.5 kHz. For frequencies above 0.6 kHz the pressure transducer output increases monotonically with respect to the microphone output. The difference peaks at about 1.5 kHz where the pressure transducer output is about 50 dB higher than the microphone output. Examining again the results of the white noise test and normalizing the pressure transducer output by the microphone output (the solid line in Fig. 5) reveals a flat response between 150 Hz and about 1 kHz. The transducer-tube system resonates at about 1.4-1.5 kHz, at ambient temperature. The SPL difference between the pressure transducer and microphone outputs is plotted in Fig. 4. It shows that at f/f_{res}=0.95 the difference is 20 dB, and a smooth line fits the data very well. The required pressure fluctuations attenuation factor was calculated using a second order polynomial fit to the inverse of the SPL difference in the form

$$Factor = -1.076\left(f/f_{res}\right)^2 + 0.1343\left(f/f_{res}\right) + 0.905 \quad (1)$$

The acoustic resonance frequency is temperature dependent and was found to scale, as expected, inversely with the square root of the temperature ratio. This point is illustrated by the additional data shown in Fig. 5. The M=0.28 and M=0.55 data were acquired outside the airfoil wake. The resonance frequencies correlate very well with the expected changes in the resonance frequency based on the tunnel flow temperature.

The experiments were conducted at Mach numbers of 0.2 to 0.65 and chord Reynolds numbers ranging from

$1.5x10^6$ to $23.5x10^6$ using the standard NACA 0012 airfoil and the NACA 0015 airfoil.

2.7 Experimental uncertainty

The incompressible experiments are conducted at conditions close to the limits of the wind tunnel operating envelope. For example, the very low temperatures (about 100K), and Mach numbers (0.28) are close to the limits of the tunnel capability. Most of the baseline data were acquired with separated regions or shock-waves present on parts of the airfoil. Tunnel wall interference will be considered at a later stage, as the tunnel wall pressures were recorded along with the airfoil and wake data. The movable walls of the test section were slightly diverged to reduce the effects of boundary layer growth. The following tables contain most of the relevant information regarding experimental uncertainties. These values were calculated using ±3 standard deviations of the various experimental conditions and calculated parameters (including repeated runs). All test instruments were calibrated prior to use.

Item	Uncertainty [% F.S.]	Full scale and condition
Slot width	5	0.5 mm
Static Temperature	0.3	300K
Static Pressure	1	70 psi, M=0.3 & 100K
R_c	2.0	M<0.3
R_c	1.0	M>0.3
M	0.5	M>0.3
F^+	1	2
$< c_\mu >$	25	local values

The uncertainty regarding the calculated airfoil aerodynamic parameters is listed in the following table (in absolute values and related to flow condition):

	fully attached	stalled	controlled
C_l	0.01	0.03	0.015
C_{dp}	0.001	0.003	0.0015
C_d	0.001	0.003	0.002

3. Discussion of results

3.1 NACA 0012 Airfoil and unsteady wake pressures

The NACA 0012 airfoil which does not contain any surface slots, and the dynamic wake rake (located at X/c=3.1 downstream of the airfoil mid-chord) were tested in order to validate the wake rake, to evaluate Reynolds and Mach number effects and to correlate the unsteady wake pressures and the airfoil pressure distributions. This section also provides guidelines for interpreting the controlled NACA 0015 data.

Figure 6a presents the lift-angle-of-attack data of the NACA 0012 for a range of Reynolds and Mach numbers. At M=0.3, a strong R_c effect is evident only up to R_c=3x10^6. At $R_c \geq 3x10^6$ and M=0.3, the maximum lift as well as post-stall lift curves are similar. A small increase of the C_l-α slope with increasing R_c can be noticed. Strong compressibility effects exist at M=0.65, compared to M=0.3, at R_c= 6x10^6. The C_l-α slope increases from 0.101 at M=0.3 to 0.133 at M=0.65 while the airfoil stalls at α lower by 7°. Compressible, post-stall lift is flat, in contradiction to the 30% lift drop observed at the incompressible stall. Strong R_c effects on the airfoil stall can be viewed in the compressible data at R_c=3x10^6 and 6x10^6.

Airfoil drag (C_d, filled symbols, solid lines) and trailing edge pressures ($C_{p,TE}$, empty symbols, broken lines) at R_c=6x10^6 and at two Mach numbers, M=0.3 and M=0.65, are plotted in Fig. 6b. The data indicate that $C_{d,0}$ is insensitive to the Mach number. The incompressible drag increases very slowly, owing to the boundary layer thickening as a result of the increased adverse pressure gradient, until $C_{l,\max}$ is reached. Then, the drag increases almost ten-fold while the lift drops by 30% (Fig. 6a). The increase in drag is accompanied by a decrease in $C_{p,TE}$ (note the inverted scale on the right hand side of Fig. 6b), which indicates the tendency to develop TE separation. Incompressible stall is accompanied by a change in the sign of $C_{p,TE}$, from positive to negative. The striking similarity between the drag and TE pressure plots demonstrates how well correlated these two quantities are in incompressible turbulent flow that is characterized by TE separation. The compressible drag divergence (Fig. 6b) occurs as a shock-wave develops over the airfoil, while the boundary layer downstream of the shock remains attached. The doubling of the compressible drag between α=5° and 6° is not accompanied by a similar increase in $C_{p,TE}$, indicating that TE separation did not develop yet. The strong shock-wave that resides over the airfoil is the main cause for the drag rise. Additionally, a local and possibly unsteady separation bubble exists downstream of the shock. The severe drag divergence occurs only between 8° and 10°, as $C_{p,TE}$ becomes negative. The measured lift and drag are close to those presented in Refs. 15 and 16. Some deviations in the stall and post stall data were identified, but are within the scatter of the data in Ref. 15.

A further demonstration of compressibility effects on the stall process of the NACA 0012 airfoil are provided by comparing airfoil pressure distributions, steady and fluctuating wake pressures, and spectra at two angles of

attack, corresponding to pre-stall and post-stall conditions with approximately the same lift coefficients.

Fig. 7a presents airfoil surface pressure coefficients at C_l=0.83 (α=8° at M=0.3 and α=6° at M=0.65). It demonstrates the distinctly different way that the compressible lift is generated versus its incompressible counterpart. While the incompressible pressure distribution contains a sharp suction peak at the LE that is followed by a steep pressure recovery, the compressible C_p indicates that the flow turns supersonic very close to the LE and ceases to accelerate at C_p≈-2.1. A strong shock-wave is located between 0.2<X/c<0.3. Downstream of X/c=0.4 the rate of pressure recovery is almost independent of the Mach number.

The wake data corresponding to C_l=0.83 is presented in Fig. 7b. The narrow mean wake at M=0.3 is accompanied by a double hump distribution of the pressure fluctuations. This shape could be attributed to the upper and lower surface boundary layers and also to a sinuous wake mode.

At M=0.65 the mean wake pressure indicates a significantly larger drag in the compressible flow, while the peak level of the wake pressure fluctuations is similar to its incompressible counterpart. The signature of the shock-wave appears in the upper section of the mean compressible wake (0<Y/c<0.15). This secondary hump in the average wake pressure deficit, is accompanied by a gradual decrease of the level of unsteadiness, indicating that the position and strength of the shock-wave are stationary.

Fig. 8 presents a comparison of the pressure distributions of the NACA 0012 airfoil at post-stall angles of attack, α=16° at M=0.3 and α=10° at M=0.65, and C_l≈0.87. The incompressible pressure distribution contains a sharp and narrow suction peak at the LE. Thereafter, it is almost flat from X/c=0.05 downstream, as the flow separates. The compressible C_p shows a supersonic flow region from the LE to X/c≈0.25 (the shock does not turn the flow subsonic) and a pressure recovery exists all the way to the TE even though the flow is separated. The effects of severe unsteadiness of the airfoil pressures on its time mean appearance are the subject of an on-going investigation.

The spectra of the wake pressures at selected points in the upper region of the wake are presented in Fig. 9. These data correspond to local maximum of p'/q (with respect to Y/c).

The frequency ordinate was normalized to present a Strouhal number based on the airfoil chord and the free stream velocity (F^+). The pressure fluctuations were corrected according to the method described in section 2.6 of the paper and frequencies above 0.95f_{res} are not presented. The data show that the spectra of the incompressible pre-stall α do not contain any distinct peak. The compressible spectra is noisier at low F^+. One possible source for the F^+=0.7 peak, measured in the wake of the M=0.65, α=6° and Y/c=0.04, is the unsteadiness of the shock-wave. A strong similarity exists between the spectra of the post-stall wakes, regardless of the Mach number. An incompressible spectral peak is found around F^+=0.25, while the compressible spectra were monotonic. At greater F^+, both post-stall spectra show a continuous decay.

4. Control of separation at compressible speeds

4.1 Overview

The main challenges of active flow control at compressible speeds are: drag reduction, delay of drag divergence, and suppression of unsteady aerodynamic loading along with its possible interaction with the structure ("buffeting"). The generation of high-lift is less important than in low Mach numbers (take-off, landing and loiter flight). Very little knowledge is available on active control of flow separation at compressible speeds. One encouraging result is reported in Ref. 17. It shows that by rotating a flat plate downstream of an airfoil experiencing shock-induced separation, the extent of separated flow could be affected. The reduced forcing frequency was close to the airfoil buffeting frequency, F^+≈0.1. These frequencies are too low for effective separation control.

There are a number of possible obstacles* to the successful application of mixing enhancement using periodic excitation to transonic flows. First, it is not clear how the excitation evolves in the supersonic flow. Second, it is not known how vorticity fluctuations are transported through shock-waves. Third, it is not clear how downstream flow modification will affect the upstream supersonic flow. Due to the many unknown aspects of the problem, it was decided to start exploring active separation control in wholly incompressible flow (M=0.28) and to gradually increase the Mach number, while maintaining constant Reynolds number, wherever possible. These flow conditions provided shock-free flow (M=0.28), a weak shock upstream of the excitation slot (M=0.4) and a strong shock-wave downstream of the slot (M=0.55). Control was applied from the slot located at X/c=10% and the excitation was of zero-mass-flux.

4.2 Separation control over the straight NACA 0015 airfoil

Fig. 10 presents the lift data of the NACA0015 airfoil at Mach numbers of 0.28 and 0.4 and at R_c=12.7x10^6. The baseline lift is presented by empty symbols and broken lines. Significant Mach number effects can be seen even at the marginally compressible flow of M=0.4.

* For brevity we list here only three important obstacles.

The baseline C_l-α slope increases by 7%, $C_{l,\max}$ drops from 1.31 to 1.17 and $\alpha_{\max}$ drops from 12° to 9°. When periodic excitation was applied to the airfoil at M=0.28, with F^+=2 and $< c_\mu >$=30x10^{-5}, stall was delayed from 12° to 14° and $C_{l,\max}$ increases from 1.31 to 1.47. When excitation was applied at M=0.4, with F^+=2.1 and $< c_\mu >$=25x10^{-5} (Fig. 10), $\alpha_{\max}$ increases from 9° to 11°, $C_{l,\max}$ increases from 1.17 to 1.29 and post-stall lift became flat. The lift increment due to the excitation is also plotted on Fig. 10. It shows that significant lift increment, due to the excitation persists as M is increased from 0.28 to 0.4. One small difference could be observed at α=8° and M=0.4, where the lift decreases slightly below the baseline as the excitation was activated.

The baseline form-drag for M=0.4 (not shown) is higher than that of the M=0.28 data, as stall is approached. The small decrease in the controlled lift prior to stall at M=0.4 (fig. 10), is accompanied by a small increase in form-drag. These detrimental effects were not observed at M<0.3.

The effect of the excitation magnitude on the airfoil lift and form-drag at M=0.28 is presented in Fig. 11. Reproducing the effects found in the low R_c experiments[3] as well as the controlled flap data at high R_c[4], the lift increases and the drag decreases proportionally to the excitation $< c_\mu >$. Saturation has not been reached at the available momentum coefficients. As indicated by the straight lines, the trends are almost logarithmic. The increased C_l-$< c_\mu >$ slope for $< c_\mu >$ > 10x10^{-5} is probably a result of increased interference with the tunnel walls. The decrease rate of form-drag is initially slower than the increase rate of the lift.

Fig. 12a presents the baseline and controlled airfoil surface pressure distributions at α=14° and M=0.28. The baseline C_p indicates that the flow separates at X/c=0.15. When excitation is applied from the slot located at X/c=0.1, the suction peak became significantly stronger and an effective pressure recovery was restored, downstream of the slot. $C_{p,TE}$ becomes more positive, indicating the increased tendency of the flow to reattach. The flow at M=0.28 is entirely subsonic, since the critical C_p (= -8.06) is not reached. Fig. 12b presents baseline and controlled pressure distributions at M=0.4 and α=11°. The baseline flow separates at X/c≈0.2. When excitation is applied, a pressure distribution similar to the one measured at M=0.28 is obtained. The only significant difference is that the upper surface flow, close to the LE, becomes supersonic as the excitation is activated ($C_{p,\text{crit}}$=-3.66). Since the flow turns subsonic again upstream of the excitation slot, one should not expect significant compressibility effects on the controlled flow.

Fig. 13a presents the steady and fluctuating wake pressure distributions measured at M=0.28, α=14° and R_c=12.7x10^6, with and without excitation. The baseline wake could not be scanned in its entirety, due to mechanical limitation on the travel of the wake rake. Therefore it had to be extrapolated in order to estimate the total drag. When a linear extrapolation was used to evaluate the baseline drag, the total drag coefficient was about 0.18. When excitation was activated the drag was reduced to 0.085. These values compare favorably with the measured reduction in form-drag, from 0.18 to 0.09, as shown in Fig. 11 for $< c_\mu >$=30x10^{-5}. The fluctuating part of the baseline wake is skewed and presents a much higher fluctuation level on the upper side, corresponding to the separated flow on the upper surface of the airfoil. A significant reduction of the wake unsteadiness was obtained due to the excitation at F^+=2. An integration of the fluctuating wake momentum, in the form

$$\frac{1}{qc}\int_{-\infty}^{\infty} p'\,dY \qquad (2)$$

indicates a reduction of 34% in the controlled flow (without extrapolating the fluctuating part of the baseline wake).

Fig. 13b presents the baseline and controlled wake pressure spectra, measured at M=0.28, α=14°, X/c=2.1 and Y/c=0.2. This position was selected because it resides where the baseline pressure fluctuations reach a maximum and dP/dY is high. It also corresponds to the airfoil upper surface, where the blowing slot is located. The baseline spectra show some peaks between F^+=0.3 to 0.7. When excitation is applied the level of the wake pressure fluctuations decreases over the entire frequency range. The most significant reduction is in the frequency range F^+<0.9. The level of the pressure fluctuations at the excitation frequency, F^+=2, is not significantly higher than the background noise in the controlled wake. This indicates that the oscillatory momentum that was introduced through the excitation slot was transferred mainly to the mean flow and also to smaller scales that dissipate rapidly in the attached regions of the turbulent boundary layer.

The global effect of the excitation frequency on the unsteadiness of the wake, as expressed in C_d excursions, can be evaluated from examining the amplitude distribution of the fundamental excitation frequency in the entire wake. Fig. 13a also presents the phase-locked pressure fluctuations measured in the wake, corresponding to the excitation frequency. It has the shape of the wake sinuous mode, which can be interpreted as alternate sign vortex shedding every half cycle from the upper and lower surfaces of the airfoil. If one assumes the theoretical shape of the phase distribution corresponding to the sinuous mode[18] and calculates the phase-locked drag excursions, it results in

only 0.6% of the controlled drag, that is lower than the baseline drag by 53%. The random wake fluctuations are assumed to average out and have no significant effect on C_d excursions. This points needs to be verified experimentally and numerically.

Data were also acquired at M=0.45 and M=0.5 at R_c=12.7x10^6 and 19x10^6. Significant R_c effects were identified in these mildly compressible flow conditions that make it difficult to identify changes in the effectiveness of the excitation. Another difficulty stems from the fact that the shock position varied but was always downstream of the fixed blowing slot (located at X/c=0.1). These results will be presented elsewhere. Here we chose to present the results for M=0.55 at R_c=19x10^6 that contain strong compressibility effects and shock position closer to X/c=0.1, but still downstream of it.

Fig. 14 presents compressible baseline and controlled lift data. It shows that the baseline $C_{l,\max}$ for M=0.55 dropped to 1 at $\alpha_{\max}$=6° from 1.31 at $\alpha_{\max}$=12° for M=0.28 (Fig. 11a) and 1.17 at 9° for M=0.4 (also in Fig. 11a). Post-stall lift decreases relative to $C_{l,\max}$, in contrast to the NACA 0012 data measured at M=0.65 and R_c=6x10^6, where post-stall lift remained fairly constant. Unlike the wholly incompressible flow, where surface tangential oscillatory excitation did not have any detrimental effect, a small decrease in lift as a result of activating the excitation can be observed at pre-stall angles of attack, at M=0.55 (note the lift change due to the excitation which is also plotted in Fig. 14). An examination of the airfoil pressure distributions (not shown) reveals that the reason for this performance degradation is a secondary shock-wave that was created at the excitation slot, upstream of the naturally occurring shock-wave. At post stall α's the excitation maintains C_l at about 1 while the baseline lift drops gradually to 0.85. As mentioned before, high lift is seldom required at transonic speeds, since the sizing of the wing is made to meet take-off requirements. The important aspects of active separation control at compressible speeds are delay the onset and alleviate the effects of buffet.

Fig. 15 presents the baseline and controlled airfoil surface pressure distributions at post-stall angle of attack (α=9°). The baseline C_p shows a supersonic flow region near the LE which turns subsonic via a strong and possibly unsteady shock-wave. The unsteadiness of the shock strength and position can be evaluated from observing the smeared foot of the shock. The average position of the shock foot is at X/c=0.15. The separated flow is manifested as a mild pressure recovery downstream of the baseline shock position and negative $C_{p,TE}$. As excitation was applied from the X/c=0.1 slot (i.e. upstream of the averaged shock position and inside the supersonic flow), a number of changes can be observed. The flow upstream of the shock accelerates. This could be a result of two possible mechanisms[19]. The excitation and the accompanied enhanced mixing thins the boundary layer upstream of the shock. In turn the boundary layer accelerates and a stronger shock is required to turn the flow subsonic again. The stronger shock also causes immediate flow separation downstream of it. The other mechanism is enhanced mixing downstream of the shock. This allows the turbulent boundary layer to close the separation bubble faster, resulting in a stronger pressure recovery and an enhanced capability to handle the stronger shock without catastrophic separation. It is assumed that both mechanisms are presently active. Indeed, the shock strength is stronger and its foot is less smeared. The pressure distribution downstream of the shock indicates that a large unsteady separation bubble exists between 0.2<X/c<0.6. A more favorable pressure recovery can be seen at X/c>0.6 and $C_{p,TE}$ becomes more positive. Clearly, the controlled flow at compressible speeds is significantly more complex than its incompressible counterpart.

The averaged and fluctuating wake pressures for M=0.55 and α=9° are presented in Fig. 16. Here also, the mechanical limitations on the movement of the wake rake prevented measurement of the entire baseline wake. The width of the wake decreased significantly, while the maximum wake deficit increased somewhat, with active excitation. This could be a result of a more stationary wake. The wake fluctuating pressure also restored a more symmetrical, double peak structure, due to the excitation. A major reduction in the wake unsteadiness can be observed on the upper side of the wake (i.e. Y/c>0).

Fig. 17a presents the drag, Fig. 17b presents the trailing edge, $C_{p,TE}$, and Fig. 17c presents the integrated wake unsteadiness as defined in Eq. 2. for the compressible baseline and controlled data. The severe drag divergence starts at α>4°, as supersonic flow turns subsonic through a strong shock-wave. The drag increases five fold (Fig. 17a) and the integrated wake unsteadiness increases six fold (Fig. 17c) between α=4° and 8°. $C_{p,TE}$ becomes negative only between α=6° and 7°, indicating the development of TE separation. The majority of the drag divergence, certainly up to 6°, was due to wave-drag and was not caused by TE flow separation.

For α≤8° the excitation results in a minor increase in drag (Fig. 17a) as well as in the wake unsteadiness (Fig. 17c), and a small but detrimental effect on $C_{p,TE}$ (Fig. 17b) . These effects accompany the pre-stall reduction in the controlled lift, observed in Fig. 14. It remains to be seen if these effects will disappear once excitation is introduced closer to or downstream of the shock-wave. For α>8° the excitation reduces the drag by about 11-17%. A similar decrease can be observed in the

integrated wake unsteadiness and in the tendency of $C_{p,TE}$ to increase due to the excitation. Again, these benefits were obtained when excitation was applied upstream of the shock position, inside the supersonic flow. The efficiency of the excitation, in terms of $< c_\mu >$, seems to be lower than in the incompressible flow conditions but it is not known what effects the passage through the shock-wave has on the vorticity of the excitation.

The spectra of the baseline and the controlled wake pressure fluctuations at α=9° are presented in Fig. 18. It demonstrates that the baseline wake at M=0.55 does not contain a distinctive shedding frequency. The controlled wake shows a reduction in the level of wake pressure fluctuations, especially in the low frequency range (F^+<1). When the level of the pressure fluctuations between 1 and 800 Hz (that includes the forcing frequency) is calculated, a reduction of about 50% is obtained (see also Fig. 16). The controlled data shows two distinctive peaks. One at F^+=1 and the other at the excitation frequency (F^+=1.65).

In order to check the effect of the wake motion on the time dependent drag excursion, we have calculated and plotted the wake pressure fluctuations, phase-locked to the excitation frequency, and the corresponding phase distribution of the fundamental excitation frequency (F^+=1.65, see Fig. 19). The amplitude and phase distributions are similar to the theoretically predicted distribution for a sinuous wake mode[18]. The phase is less coherent on the upper edge of the wake, corresponding to the controlled flow, but the shape is close to the theoretical prediction and to experiments. The phase-locked C_d excursions are calculated using the mean wake profile with the amplitude and phase distributions superimposed. We found that the C_d excursions are less than 0.3%, compared to 11% drag reduction which is obtained due to the excitation. Here also, the reduction in C_d excursions needs to be validated by unsteady airfoil surface pressures and balance data.

Fig 20 presents the improvement in the airfoil integral parameters as the excitation magnitude, $< c_\mu >$, is increased, at M=0.55 and α=9°. The data shows that the relative lift to drag ratio increases by 35%, in an almost linear manner with the increase in $< c_\mu >$. This trend is highly desirable for the construction of a linear controller. The wake gradually becomes steadier as the lift to drag ratio increases as a result of increased excitation magnitude. The averaged pressure gradient downstream of the active excitation slot increased by 50% and $C_{p,TE}$ increased by 30% due to the excitation with F^+=1.65 and $< c_\mu >$=0.015% (not shown). This indicates that the above benefits were obtained as a result of an increased tendency for flow reattachment.

5. Conclusions

Active separation control was applied from the leading edge region of a straight NACA 0015 airfoil, initially in incompressible flow. Then the Mach number was gradually increased to cover compressible flows at flight Reynolds numbers.

Strong Reynolds number effects were identified in the airfoils baseline performance at moderately compressible flow conditions and post stall angles of attack. It makes the identification of clear trends in the controlled data difficult. The R_c effects weaken as the Mach number increases and a stronger shock develops.

It was demonstrated, in accordance with low Reynolds number experiments, that incompressible $C_{l,\max}$ can be increased by 15%, post-stall lift can be increased by as much as 50% and post stall drag can be reduced by more than 50%. The controlled wake is also steadier. The main application of the present control method to these flow conditions is a reduction in the number of elements and their complexity in high-lift systems while maintaining the performance and steady flow. These benefits should allow simpler and lighter high-lift systems.

The significant increase in lift and lift to drag ratio, obtainable in incompressible speeds, should not be expected at compressible speeds. The global effect of the method is to accelerate the upstream boundary layer due to the delay of boundary layer separation. In compressible speeds this could lead to a stronger shock-wave that in turn causes a more severe separation, that is harder to control. This process saturates the effect. Also at increased Mach number the required frequencies increase at least linearly with the flow speed while the available $< c_\mu >$ is inversely proportional to the dynamic pressure. In transonic flow, the method could be used to alleviate buffet rather than generating higher lift.

When excitation was applied well upstream of the shock-wave it had a detrimental effect on lift, drag and wake steadiness. This is due to the creation of a secondary shock-wave at the blowing slot. This effect is not present in low Mach number experiments. There, the introduction of wall-tangential excitation, far upstream of the boundary layer separation, resulted in a *smaller performance increment* (when compared to excitation that was introduced immediately upstream of the separation), but did not result in absolute *performance degradation*.

It seems that the ability of similar $< c_\mu >$ levels to reduce drag and wake unsteadiness decreases as M increases. But due to the great sensitivity of the blowing slot location with respect to the mean shock position, it remains to be seen how the efficiency will vary once this parameter is better controlled.

The excitation became effective when it was introduced only slightly upstream of the shock-wave,

increasing the lift-to-drag ratio, reducing the drag and causing a steadier wake. C_d excursions due to phase-locked wake pressure fluctuations at the excitation frequency were smaller than 1% of the controlled C_d, while the drag reduction was 53% at M=0.28 and 11-17% at M=0.55.

The excitation frequency, F^+, and its magnitude, $< c_\mu >$, should be selected and tested with respect to the target of the control strategy. These could be increased lift, increased L/D, reduced drag, and reduced broad or narrow band wake unsteadiness. A strong sensitivity of C_l, C_d and wake unsteadiness on $< c_\mu >$ was identified. Specifically, three regimes are noted: low effectiveness due to lower than threshold ($< c_\mu >$ < 0.001% in compressible flow), increasing effectiveness with increasing $< c_\mu >$, saturation in C_l and C_d and increased unsteadiness due to overwhelmingly high excitation ($< c_\mu >$ > 0.1%, not reached in the present experiment).

Specifically, it could safely be stated that whenever controlled excitation was applied close enough to the separation location, it proved beneficial, regardless of the Mach number.

Closed-loop control could be applied to minimize C_p, form drag or moment excursions using proper instrumentation and control strategy. Many of the open aspects of the control of flow separation mentioned above are presently under investigation.

Acknowledgment

This work was performed while the first author held a National Research Council - NASA LaRC research associateship. The authors would like to thank Mr. W. L. Sellers III, Mr. M. Walsh, Dr. R. Joslin, Ms. C.B. McGinley, Dr. J. F. Barthelemy and Dr. R. W. Wlezien for the continuous support. The authors would also like to thank Mr. B.K. Stewart and the entire 0.3mTCT crew from LaRC, for the support.

References

1. Gad-el-Hak, M. and Bushnell, D.M., "Separation control: Review", *J. of Fluids Eng*., Vol. 113, March 1991, pp. 5-30.
2. Seifert, A., Bachar, T., Koss, D., Shepshelovich, M. and Wygnanski, I., "Oscillatory blowing, a tool to delay boundary layer separation", *AIAA J.*, Vol. 31, No. 11, Nov. 1993, pp. 2052-2060.
3. Seifert, A., Darabi, A. and Wygnanski, I. "On the delay of airfoil stall by periodic excitation", *AIAA J. of Aircraft*. Vol. 33, No. 4 , July-August 1996, pp. 691-699.
4. Seifert, A. and Pack, L.G., "Oscillatory control of separation at high Reynolds numbers" AIAA paper 98-0214, 1998. Submitted to *AIAA Journal*.
5. Wu, J.Z., Lu, X.Y., Denny, A.G, Fan, M. and Wu, J.M., "Post-Stall Flow Control on an Airfoil by Local Unsteady Forcing", *J. Fluid Mech*., vol. 371, pp. 21-58, 1998.
6. Donovon, J.F., Kral, L.D. and Cary, A.W., "Active flow control applied to an airfoil", AIAA paper 98-0210, 36th Aerospace Sciences meeting, Jan. 12-15, 1998, Reno, NV.
7. Delery, J.M., "Shock Wave/Turbulent Boundary Layer Interaction and its Control", *Prog. In Aerospace Sci.* Vol. 22, pp. 209-280, 1985.
8. McCormick, D.C., "Shock-Boundary Layer Interaction with Low Profile Vortex Generators and Passive Cavity", AIAA paper 92-0064, 30th Aerospace Sciences meeting, Jan. 6-9, 1992, Reno, NV.
9. Wallis, R.A and Stuart, C.M., "On the Control of Shock-induced Boundary-Layer Separation with Discrete Air Jets", A.R.C. C.P. number 595, 1962.
10. Mounts, J.S. and Barber, T.J., "Numerical Analysis of Shock-Induced Separation Alleviation Using Vortex Generators", AIAA paper 92-0751, 30th Aerospace Sciences meeting, Jan. 6-9, 1992, Reno, NV.
11. Krogmann, P. and Stanewsky, E., "Effects of Local Boundary Layer Suction on Shock-Boundary Layer Interaction and Shock-Induced Separation", AIAA paper 84-0098, 22nd Aerospace Sciences meeting, Jan. 9-12, 1984, Reno, NV.
12. Scott, M.A., Montgomery, R.C. and Weston, R.P., "Subsonic maneuvering effectiveness of high performance aircraft which employ quasi-static shape changes devices", Presented at the 36th SPIE, Smart structures and materials, San Diego, CA, March 1998.
13. Rallo, R. A., Dress, D.A. and Siegle, H. J. A., "Operating Envelope Charts for the Langley 0.3-meter Transonic Cryogenic Wind Tunnel", NASA TM-89008, 1986.
14. Ladson, C. A. and Ray, E. J., "Evolution, Calibration, and Operational Characteristics of the Two-dimensional Test Section of the Langley 0.3-meter Transonic Cryogenic Tunnel", NASA TP-2749, 1987.
15. McCroskey, W.J., "A Critical Assessment of Wind Tunnel Results for NACA 0012 Airfoil", NASA TM 100019, 1987.
16. Ladson, C.L. and Hill, A.S., "High Reynolds Number Transonic Tests of an NACA 0012 Airfoil in the Langley 0.3 m Transonic Cryogenic Tunnel", NASA TM 100527, 1987.
17. Szumowski, A.P. and Meier, G.E.A., "Forced Oscillations of Airfoil Flows", *Experiment in Fluids*, Vol. 21, 1996, pp. 457-464.
18. Marasly, B, Champagne, F.H. and Wygnanski, I., "Effects of travelling wave on the growth of a turbulent wake", *J. Fluid Mech*, 235, 1991, pp. 511-528.
19. Chang, P. K., "Separation of Flow", Perganon Press, 1970, p. 227-228.

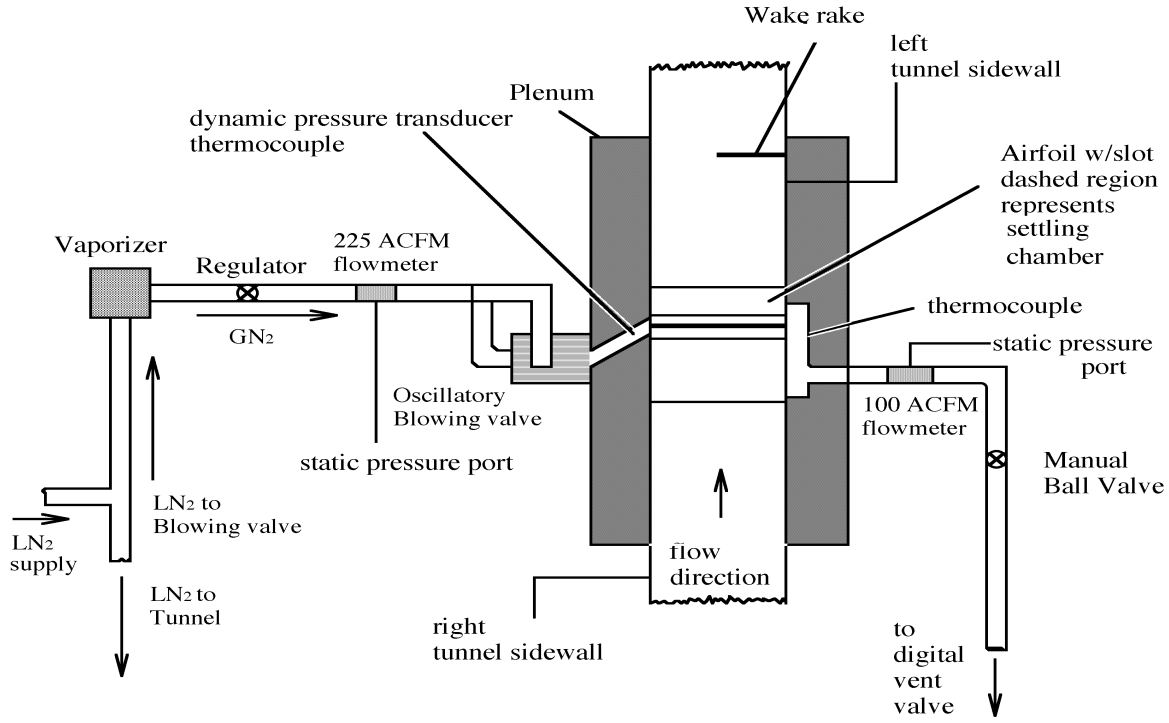

Fig. 1 A schematic description of the experimental set-up in the 0.3m Transonic Cryogenic Tunnel wind (top view).

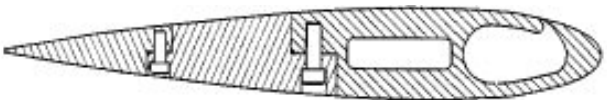

Fig. 2 NACA 0015 airfoil with a blowing slot at X/c=10%.

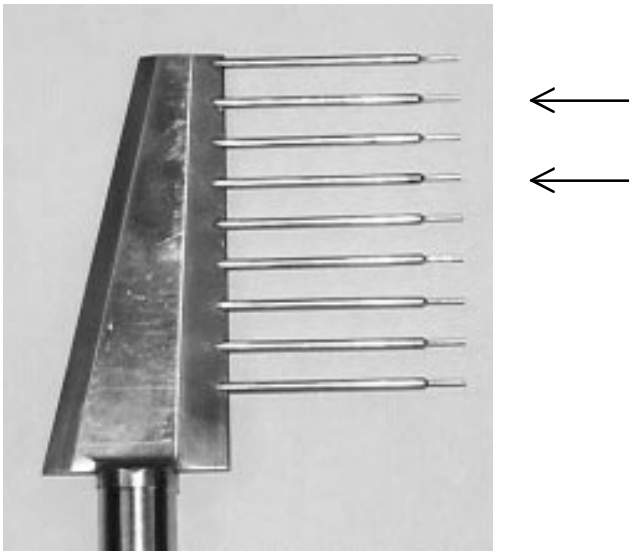

Fig. 3 The wake-rake with dynamic pressure transducers (arrows indicate instrumented tubes), tube spacing: 12.7mm.

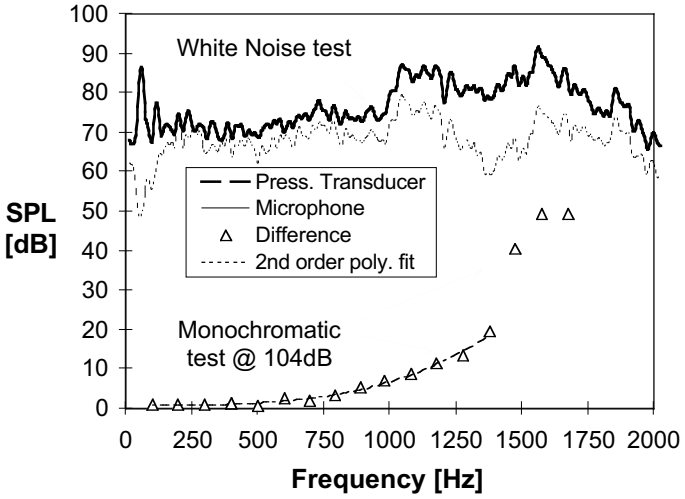

Fig. 4 Frequency response of the dynamic wake-rake .

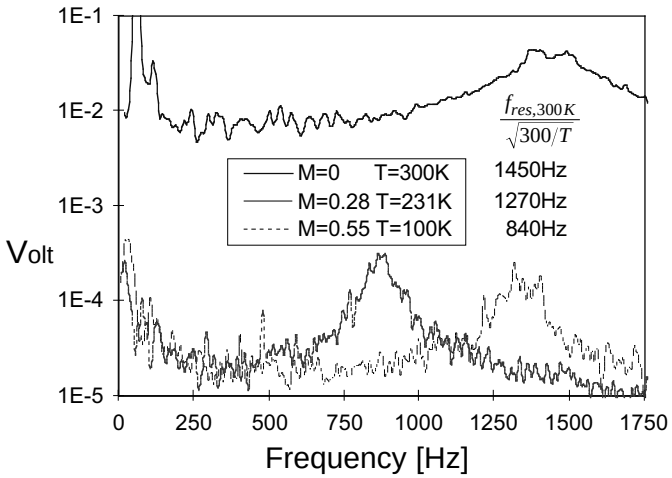

Fig. 5 Temperature effect on the resonance of the transducer-tube system of the dynamic wake-rake .

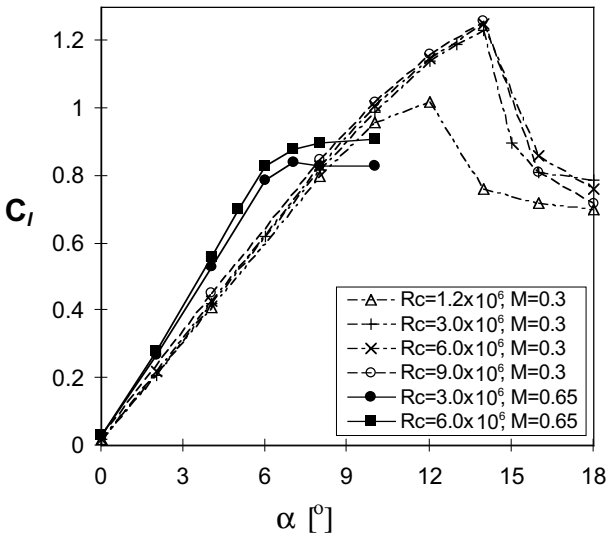

Fig.6a Mach and Reynolds number effects on the lift of the NACA 0012 airfoil.

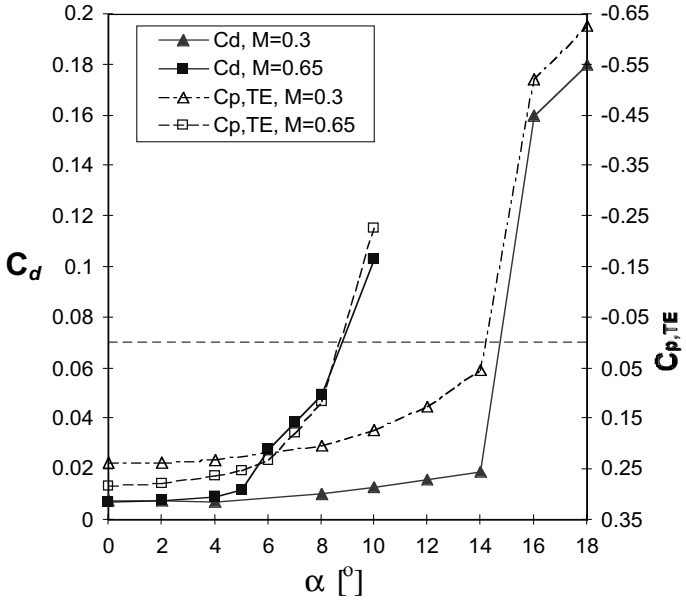

Fig.6b Drag and TE pressure of the NACA 0012 airfoil, R_c=6.0x10^6.

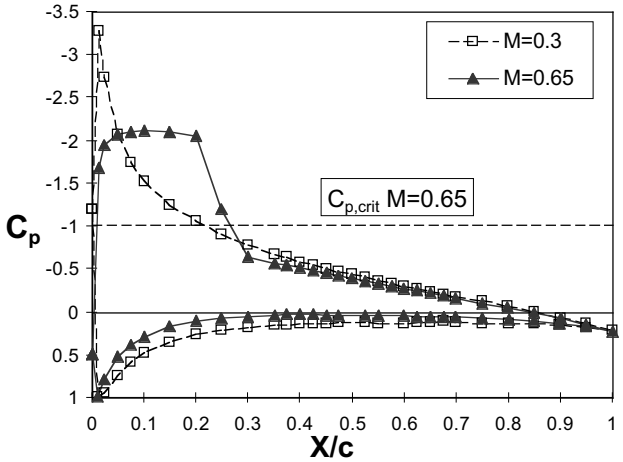

Fig. 7a NACA 0012 pressure coefficients. R_c=6.0x10^6 C_l=0.83, α=8° (M=0.3) and 6° (M=0.65).

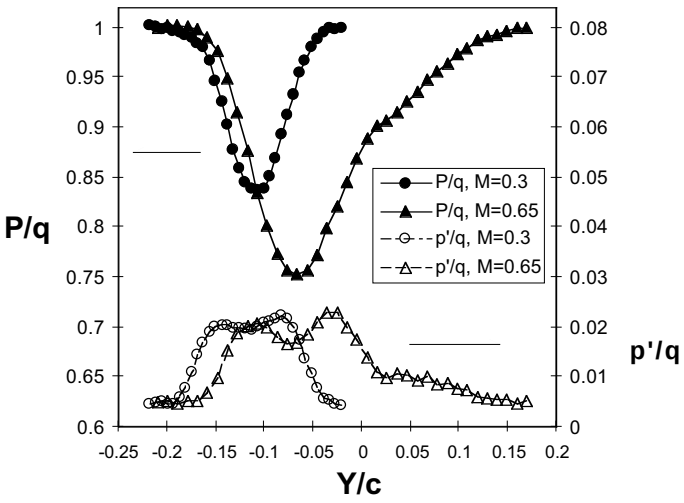

Fig. 7b NACA 0012 mean and fluctuating wake pressures. R_c=6.0x10^6, α=8° (M=0.3) and 6° (M=0.65).

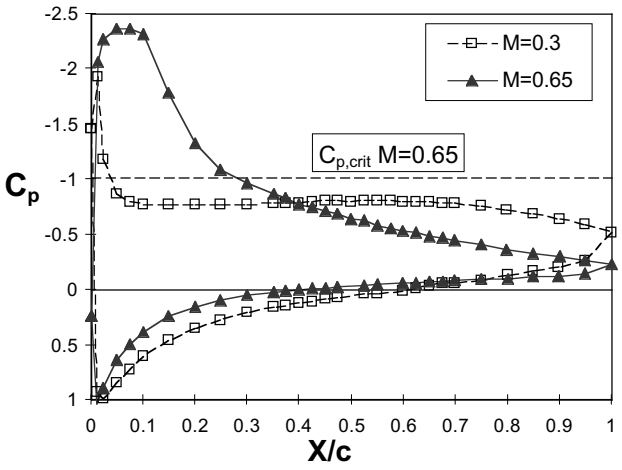

Fig. 8 NACA 0012 pressure coefficients. R_c=6.0x10^6 C_l=0.87, α=16° (M=0.3) and 10° (M=0.65).

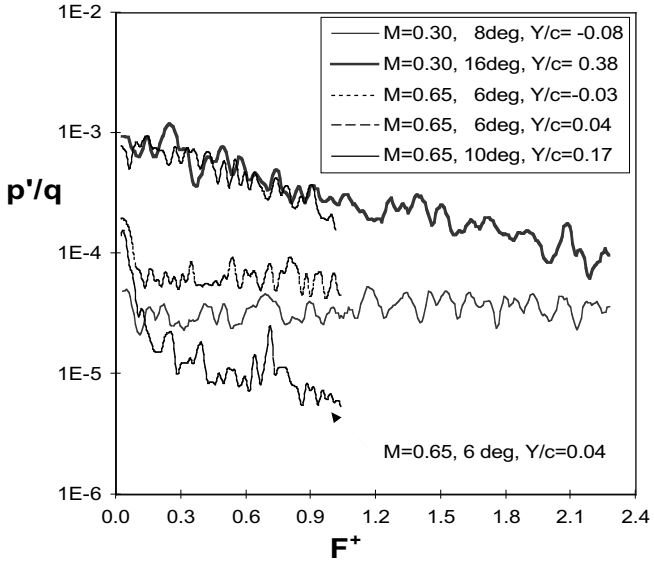

Fig. 9 NACA 0012 pressure spectra. R_c=6.0x10^6, α in legend.

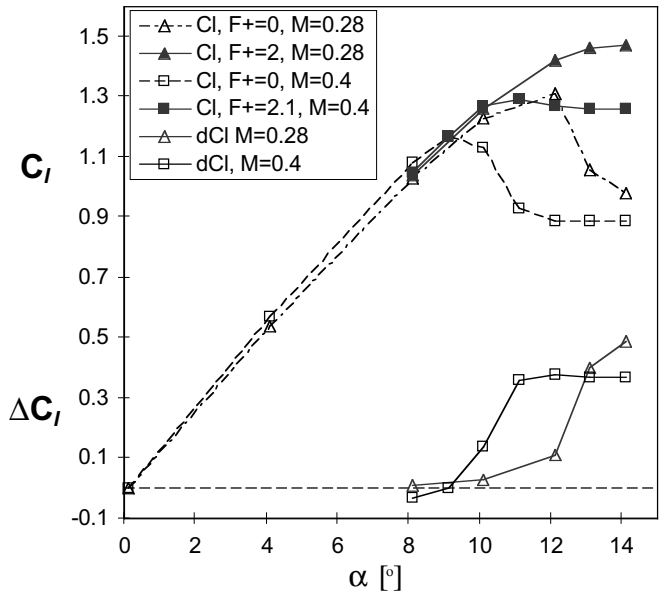

Fig.10 The effects of Mach number and periodic excitation on the lift of the NACA 0015 airfoil. R_c=12.7x10^6, <cμ>=0.03% (M=0.28) and 0.025% (M=0.4).

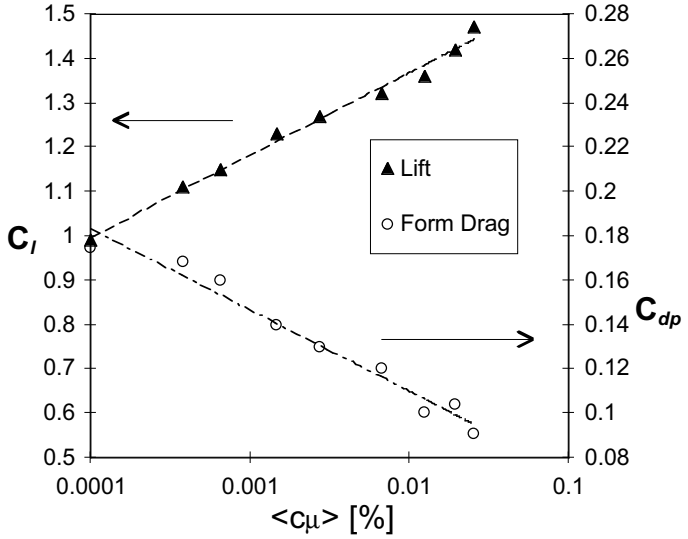

Fig.11 The effects of excitation magnitude on the performance of the NACA 0015 airfoil. α=14°, M=0.28, R_c=12.7x10^6.

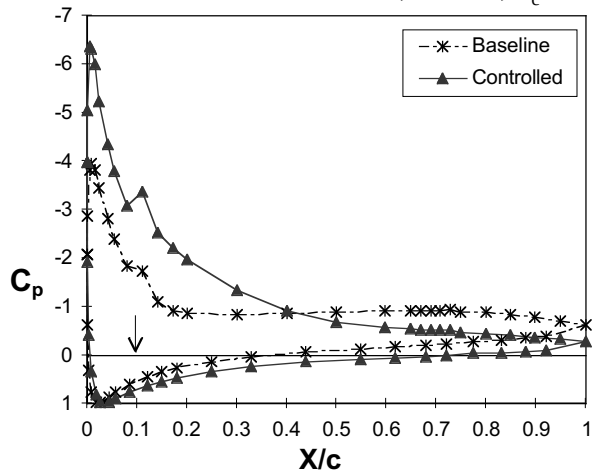

Fig. 12a NACA 0015 pressure coefficients. M=0.28 , α=14^0 R_c=12.7x10^6, F^+=2, <cμ>=0.03%. Arrow indicates blowing slot

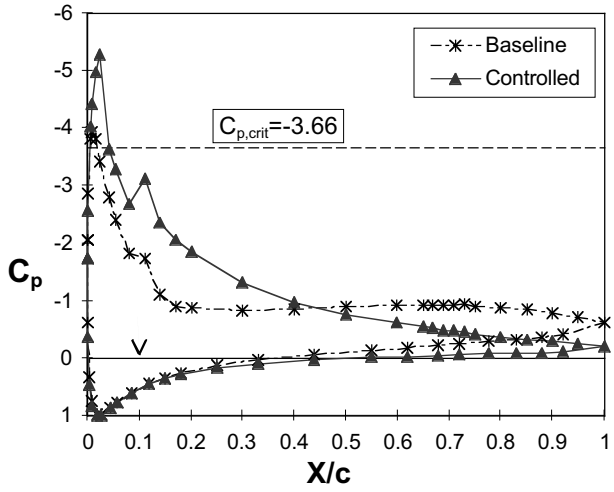

Fig. 12b NACA 0015 pressure coefficients. M=0.4 , α=11^0 R_c=12.7x10^6, F^+=2, <cμ>=0.025%. Arrow indicates slot.

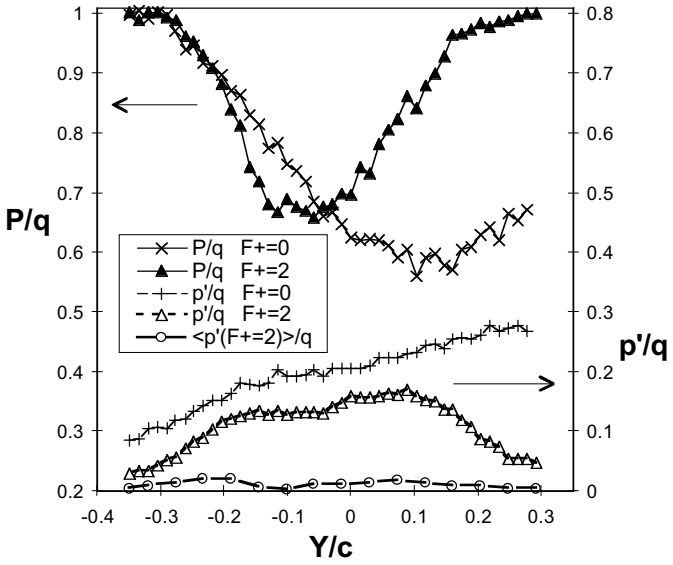

Fig. 13a NACA 0015 total, fluctuating and phase-locked wake pressures. R_c=12.7x10^6, α=14^0, M=0.28 , <cμ>=0.03%.

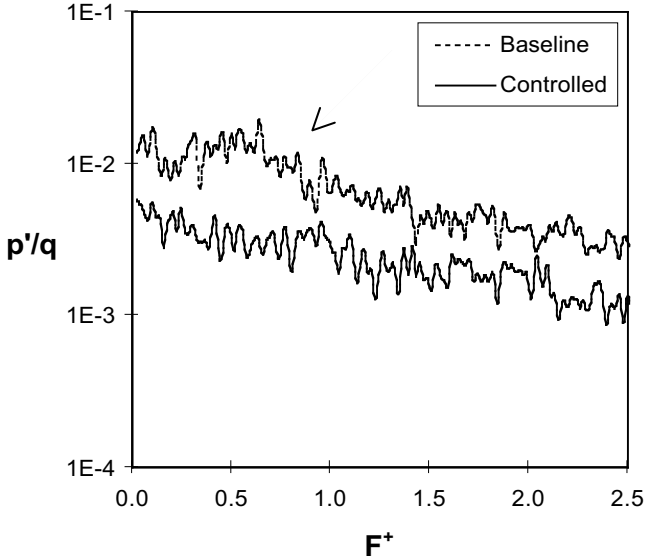

Fig. 13b Pressures spectra, conditions as in Fig. 13a, Y/c=0.2

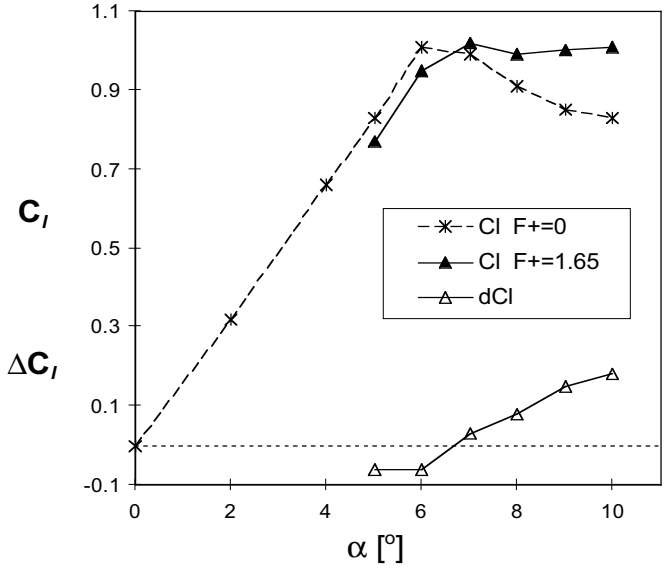

Fig.14 The effects of periodic excitation on lift of the NACA 0015 airfoil. R_c=19x10^6, M=0.55, <cμ>=0.015%.

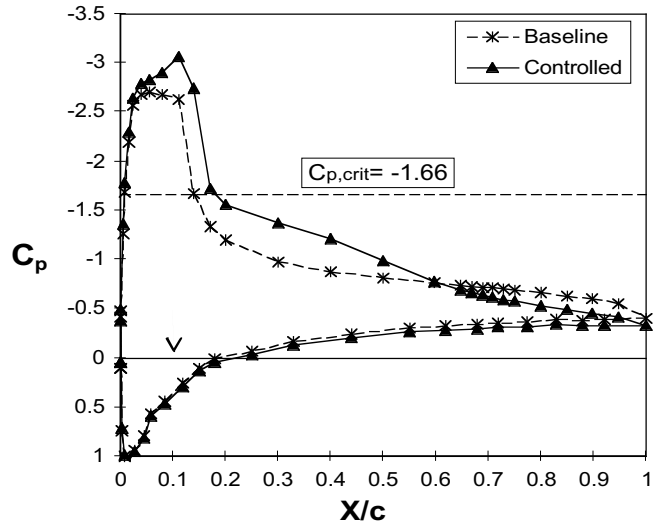

Fig.15 Baseline and controlled airfoil pressures. R_c=19x10^6, M=0.55, , α=9^0, F$^+$=1.65, <cμ>=0.015%. Arrow indicates slot.

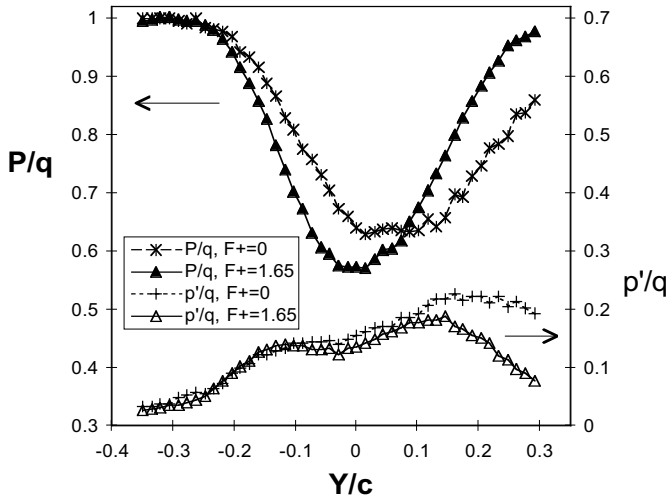

Fig.16 Baseline and controlled wake pressures. R_c=19x10^6, M=0.55, , α=9^0, F$^+$=1.65, <cμ>=0.015%.

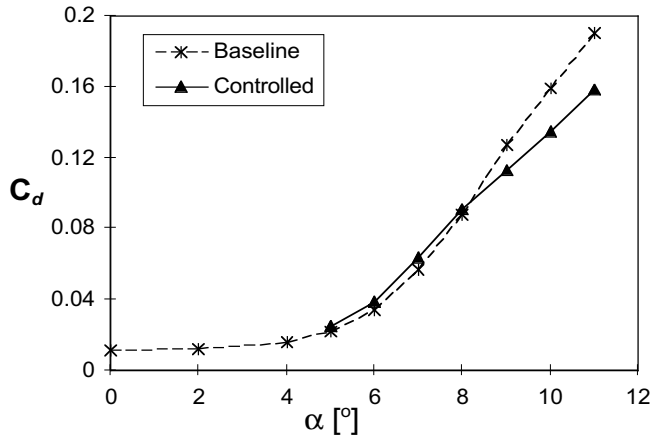

Fig.17a Baseline and controlled airfoil drag. R_c=19x10^6, M=0.55, F$^+$=1.65, <cμ>=0.015%.

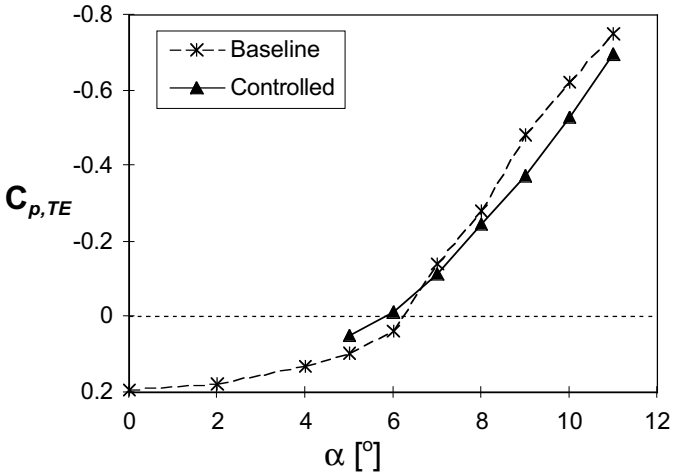

Fig.17b Baseline and controlled airfoil TE pressure. R_c=19x10^6, M=0.55,, F$^+$=1.65, <cμ>=0.015%.

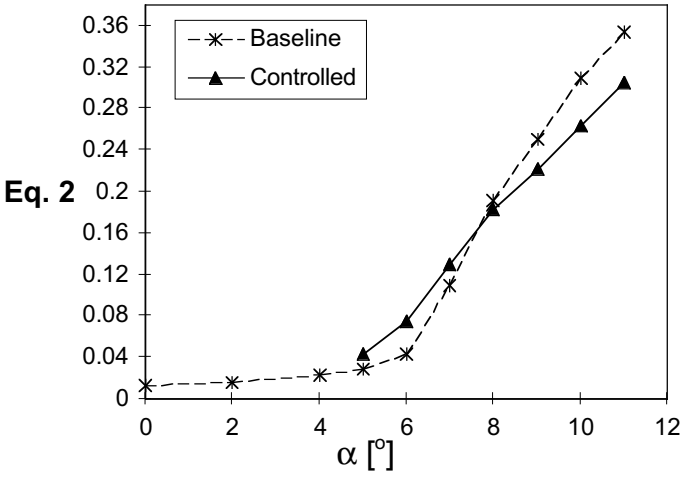

Fig.17c Baseline and controlled wake unsteadiness. R_c=19x10^6, M=0.55,, F$^+$=1.65, <cμ>=0.015%.

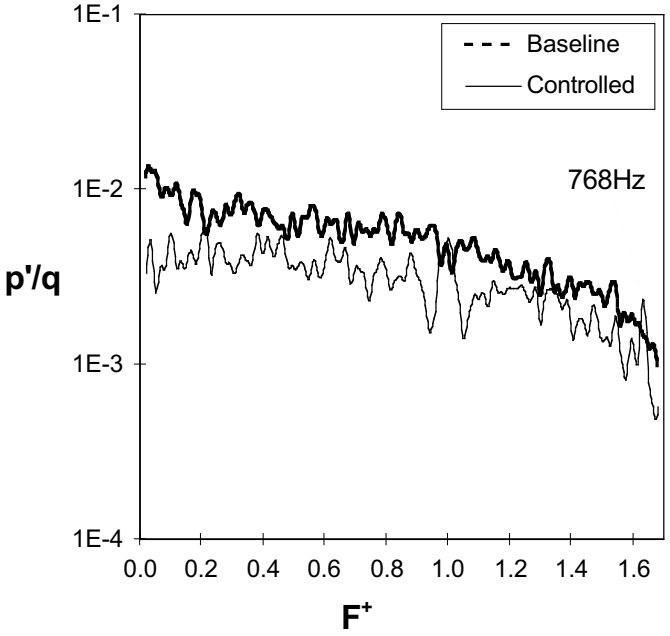

Fig.18 Baseline and controlled wake spectra. $R_c=19x10^6$, M=0.55, Y/c=0.25, $\alpha=9^0$, $F^+=1.65$, $<c\mu>=0.015\%$.

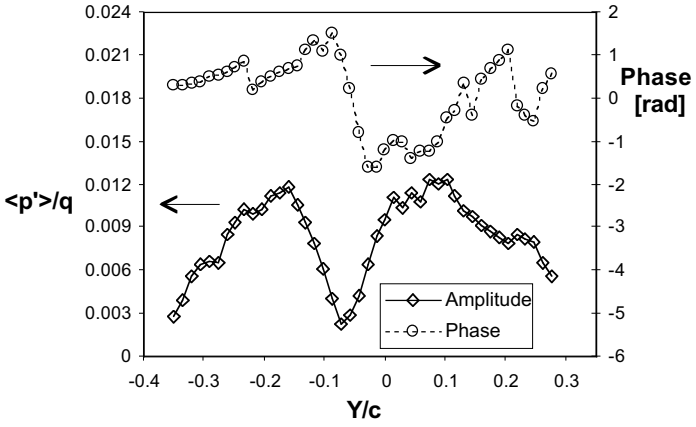

Fig.19 Amplitude and phase distributions at the excitation Frequency. Corresponding to the data of Fig. 16. M=0.55.

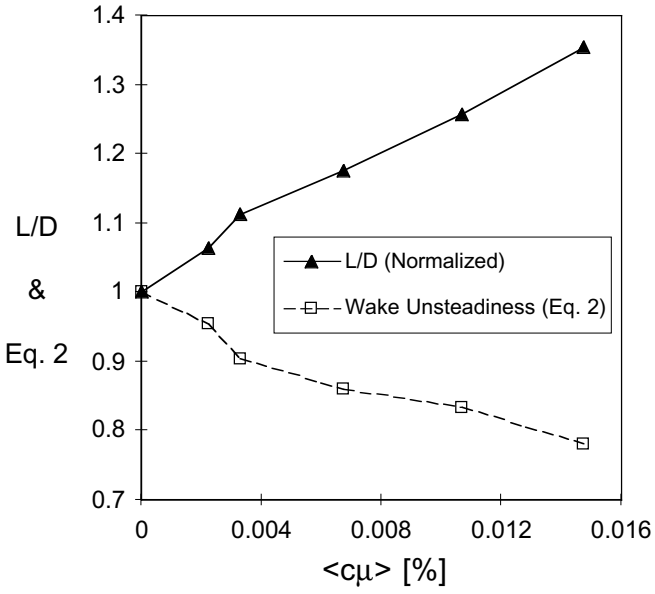

Fig. 20 Baseline and controlled airfoil lift to drag ratio and Integrated wake unsteadiness vs excitation magnitude, both normalized by their baseline values. $R_c=19x10^6$, M=0.55, $F^+=1.65$, $\alpha=9^0$.